*Journal of Biomolecular Structure and Dynamics*, 2016
Vol. 34, No. 4, 705–715, http://dx.doi.org/10.1080/07391102.2015.1055303

Taylor & Francis
Taylor & Francis Group

# The systematic approach to describing conformational rearrangements in G-quadruplexes

Vladimir Tsvetkov[a,b]*, Galina Pozmogova[a] and Anna Varizhuk[a,c]*

[a]*Department of Molecular Biology and Genetics, SRI of Physical-Chemical Medicine, Moscow, 119435, Russia;* [b]*Department of Polyelectrolytes and Surface-active Polymers, Topchiev Institute of Petrochemical Synthesis, Moscow, 119991, Russia;* [c]*Department of Structure-Functional Analysis of Biopolymers, Engelhardt Institute of Molecular Biology, Vavilov str. 32, Moscow, 119991, Russia*

Communicated by Ramaswamy H. Sarma

(*Received 21 January 2015; accepted 22 May 2015*)

Conformational changes in DNA G-quadruplex (GQ)-forming regions affect genome function and, thus, compose an interesting research topic. Computer modelling may yield insight into quadruplex folding and rearrangement, particularly molecular dynamics simulations. Here, we show that specific parameters, which are distinct from those commonly used in DNA conformational analyses, must be introduced for adequate interpretation and, most importantly, convenient visual representation of the quadruplex modelling results. We report a set of parameters that comprehensively and systematically describe GQ geometry in dynamics. The parameters include those related to quartet planarity, quadruplex twist, and quartet stacking; they are used to quantitatively characterise various types of quadruplexes and rearrangements, such as quartet distortion/disruption or deviation/bulging of a single nucleotide from the quartet plane. Our approach to describing conformational changes in quadruplexes using the new parameters is exemplified by telomeric quadruplex rearrangement, and the benefits of applying this approach to analyse other structures are discussed.

**Keywords:** nucleic acid conformations; G-quadruplexes; molecular modelling

## Introduction

Much research in the fields of molecular biology and biophysical chemistry is devoted to noncanonical nucleic acid structures. Conformational rearrangements in G-quadruplexes (GQs), which are planar arrays of guanine tetrads paired by Hoogsteen bonding, are particularly important because they may account for multiple transcription/translation/recombination and splicing-related events (Bochman, Paeschke, & Zakian, 2012; Burge, Parkinson, Hazel, Todd, & Neidle, 2006; Maizels, 2006; Murat & Balasubramanian, 2014). Molecular modelling is commonly used to complement NMR and XRD data on known GQ structures or to predict rearrangements in GQs upon interaction with various ligands (Haider & Neidle, 2010; Šponer, Cang, & Cheatham, 2012). A number of software packages and web servers, including VMD (Humphrey, Dalke, & Schulten, 1996), CURVES (Blanchet, Pasi, Zakrzewska, & Lavery, 2011), 3DNA (Colasanti, Lu, & Olson, 2013) and some others, allow for visualisation of noncanonical nucleic acid structures and the assessment of basic structural parameters. However, specific parameters are necessary to quantitatively describe GQ geometry. Ideally, such parameters should aid in characterising various types of GQ topologies in dynamics. Basic parameters, such as backbone torsion angles, glycosidic torsion angles and sugar pucker, are informative and applicable to flexibility characterisation (Cang, Sponer, & Cheatham, 2011; Li, Luo, Xue, & Li, 2010) but not GQ characterisation. Similarly, the traditional root mean square deviations (RMSD) assessment cannot be used to comprehensively characterise GQ conformational fluctuations as a function of time. Several researchers have attempted to introduce GQ-specific parameters, but a systematic study has not been reported.

Lech et al. described stacked G-tetrad geometry using two specific parameters in a study on the influence of stacking on GQ stability: relative rotation angle and the distance between parallel planar tetrads (separation distance). For opposite-polarity-stacked tetrads, the angle between stacked tetrads was defined as the rotation of one tetrad in the direction of its hydrogen bond polarity with respect to another tetrad through the central axis that is perpendicular to the tetrad plane. For same-polarity-stacked tetrads, the angle was arbitrarily defined as the rotation of the tetrad containing the 5′-end guanine in the direction of its hydrogen bond polarity (Lech, Heddi, & Phan, 2013). Both the rotation angle (also referred to as the "twist angle") and separation distance are key characteristics of GQs, and their fluctuations indicate conformational changes in GQs. For example, twist angle time plots have been used to monitor dynamics of the thrombin-binding GQ aptamer (TBA) (Reshetnikov,

*Corresponding authors. Email: v.b.tsvetkov@niifhm.ru (V. Tsvetkov); annavarizhuk@niifhm.ru (A. Varizhuk)

Golovin, Spiridonova, Kopylov, & Šponer, 2010) (the twist angle was determined as the angle between the vectors that join adjacent guanine C1′ atoms in each of the two TBA tetrads). In another recent TBA modelling study (Reshetnikov, Golovin, & Kopylov, 2010), a more in-depth analysis of GQ dynamics was performed, and two original parameters were reported. The distance between the G-quartet guanine centres of mass (COMs) was used to monitor "in plane" GQ motions (fluctuations in a quartet plane), and the distance between the two tetragon COMs (the outer tetragon was formed by the N9 atoms, and the inner tetragon formed by the O6 atoms) was used to monitor "out of plane" GQ motions (the tendency of a quartet to form a tepee structure). An alternative approach to assessing "out of plane" GQ motions was proposed by Zhu, Xiao, and Liang (2013). They demonstrated G-tetrad deviation from the plane conformation in telomeric GQs using RMSD for the axis perpendicular to the tetrad plane. Additional specific parameters have been introduced to describe conformational changes in GQ loops (Zhu et al., 2013) and ion capture (Reshetnikov et al., 2011), but those types of changes are outside the scope of this article.

The above studies were not aimed at comprehensive GQ characterisation but were focused on different individual aspects of GQ conformational diversity and dynamics. We analysed and reconsidered the approaches used in those studies to propose an original set of parameters for monitoring GQ quartet planarity and integrity. Relative orientation of GQ quartets can be characterised using known parameters (Lech et al., 2013), i.e. twist angle and separation distance. Fluctuations of the new parameters indicate both "in plane" and "out of plane" GQ motions and may be used to monitor GQ distortion/disruption or single-nucleotide bulging. The latter type of GQ rearrangement has not been quantitatively analysed so far, but it is important given the recently reported new types of quadruplexes (Mukundan & Phan, 2013).

Herein, we use a model of the human telomeric quadruplex (telGQ) to illustrate the advantages of our new parameters in describing various types of motions because telGQ is a well-characterised structure, and its folding as well as unfolding pathways have been investigated in detail (Gray, Trent, & Chaires, 2014; Lane, Chaires, Gray, & Trent, 2008; Stadlbauer, Trantírek, Cheatham, Koča, & Šponer, 2014). Human telomere sequences can adopt different topologies, including an anti-parallel basket structure with one diagonal and two lateral loops (Wang & Patel, 1993), a parallel structure with all strand-reversal loops (Parkinson, Lee, & Neidle, 2002), [3+1] hybrid structures with one strand-reversal and two lateral loops (Luu, Phan, Kuryavyi, Lacroix, & Patel, 2006; Phan, Luu, & Patel, 2006) and certain higher-order structures (Petraccone et al., 2011). In a $K^+$ solution, natural human telomere fragments comprising four G tracks and one- or two-nucleotide flanks are slowly exchanging conformers of the hybrid GQ, "hybrid-1" and "hybrid-2." The conformers differ in the loop arrangement (Phan et al., 2006), and their ratio depends on the flanks; d[TAGGG(TTAGGG)$_3$] forms up to 70% of hybrid-1 (PDB entry 2JSM), and d[TAGGG(TTAGGG)$_3$TT] forms up to 70% of hybrid-2 (PDB entry 2JSL). In d[TAGGG(TTAGGG)$_3$T], the two conformers form at comparable proportions (Phan, Kuryavyi, Luu, & Patel, 2007).

We also discuss a TBA analogue (the thrombin-binding aptamer with a non-natural (triazole) internucleotide linkage) to demonstrate that the new parameters also apply to modified and artificial GQ structures.

We report explicit solvent and implicit solvent molecular dynamics simulations (MD) for the TBA analogue and the telomeric GQ, respectively. The MD trajectories are relatively short because we did not mean to ascertain the conformations of the already known TBA and telGQ structures – we rather use them as model GQs. The systematic approach described herein and the new parameters can be employed for interpretation and convenient visual representation of any simulations of GQ dynamics.

## Materials and methods

We modelled a telGQ hybrid-1 (d[TAGGG(TTAGGG)$_3$]; PDB: 2JSM) in implicit solvent and a TBA analogue with a triazole internucleotide linkage (d[GGTTGGTT*TGGTTGG], where * is a modified fragment; for schematic representation, see Supplementary material) in explicit solvent ($T = 300$ K; the negative charges were neutralised by adding $Na^+$ ions, and $K^+$ ions were used to stabilise the triazole–TBA GQ structure) with the Amber 10 suite. Two models of the triazole–TBA complex with thrombin were obtained using the NMR-based and XRD-based models of the TBA/thrombin complex (PDB entries 1HAO and 1HUT, respectively). For more information and the details of the explicit solvent MD simulation, see (Varizhuk et al., 2013). Implicit solvent MD simulation of telGQ was performed as follows.

The conditions described in (Varizhuk et al., 2013) did not yield substantial conformational rearrangements in the telomeric GQ, and therefore, we increased the temperature to facilitate the rearrangements ($T = 400$ K). Implicit solvent in generalised Born/solvent-accessible surface area (GB/SA) formalism (Bashford & Case, 2000) was employed using the OBC application developed by Onufriev, Bashford, and Case (2000) in the presence of 0.1 M NaCl. The DNA interatomic interactions were calculated using a parmbsc0 force field. Prior to MD simulation, the model structure was minimised by 250 steps of steepest descent followed by 250 steps of conjugate gradient. Next, gradual heating to 400 K over 20 ps was performed. The SHAKE algorithm (Ryckaert,

Ciccotti, & Berendsen, 1977) was applied to constrain the hydrogen atom bonds, which allowed us to use a 2 fs step. The dielectric constants 1 (interior) and 80 (exterior) were employed in the GB-MD simulations. The production phase of the GB-MD simulations continued until the quadruplex core was disrupted (approximately 34 ns). To control the temperature, we used the Langevin thermostat with the collision frequency 5 $ps^{-1}$. Snapshot visualisation and conformational rearrangement analyses were performed using VMD program. Snapshots were collected every 0.1 ns. The new GQ-related parameters were calculated using programs written with the internal VMD atom selection language. To conveniently represent the parameter plots, short-term fluctuations were smoothed by the moving average method (the span for the moving average was five).

## Results and discussion

### *GQ-related parameters: general description*

We developed a set of parameters that facilitate comprehensive quantitative characterisation of potentially any GQ core in dynamics. A schematic representation of the hybrid-1 telGQ core is shown in Figure 1(A) as an illustration of our numeration system. We used core-related numeration, which is independent from loop arrangement and does not coincide with numeration along the chain, but is universal and convenient for indexing parameters. Quartet numeration begins at the 5′-terminus. The guanines in the 1st quartet are numbered in the direction of the hydrogen bonding polarity, from the donor to the acceptor, and from the 5′-terminus. In the case of telGQ, the direction is counterclockwise from the perspective of the 1st quartet. The guanines in other quartets are numbered

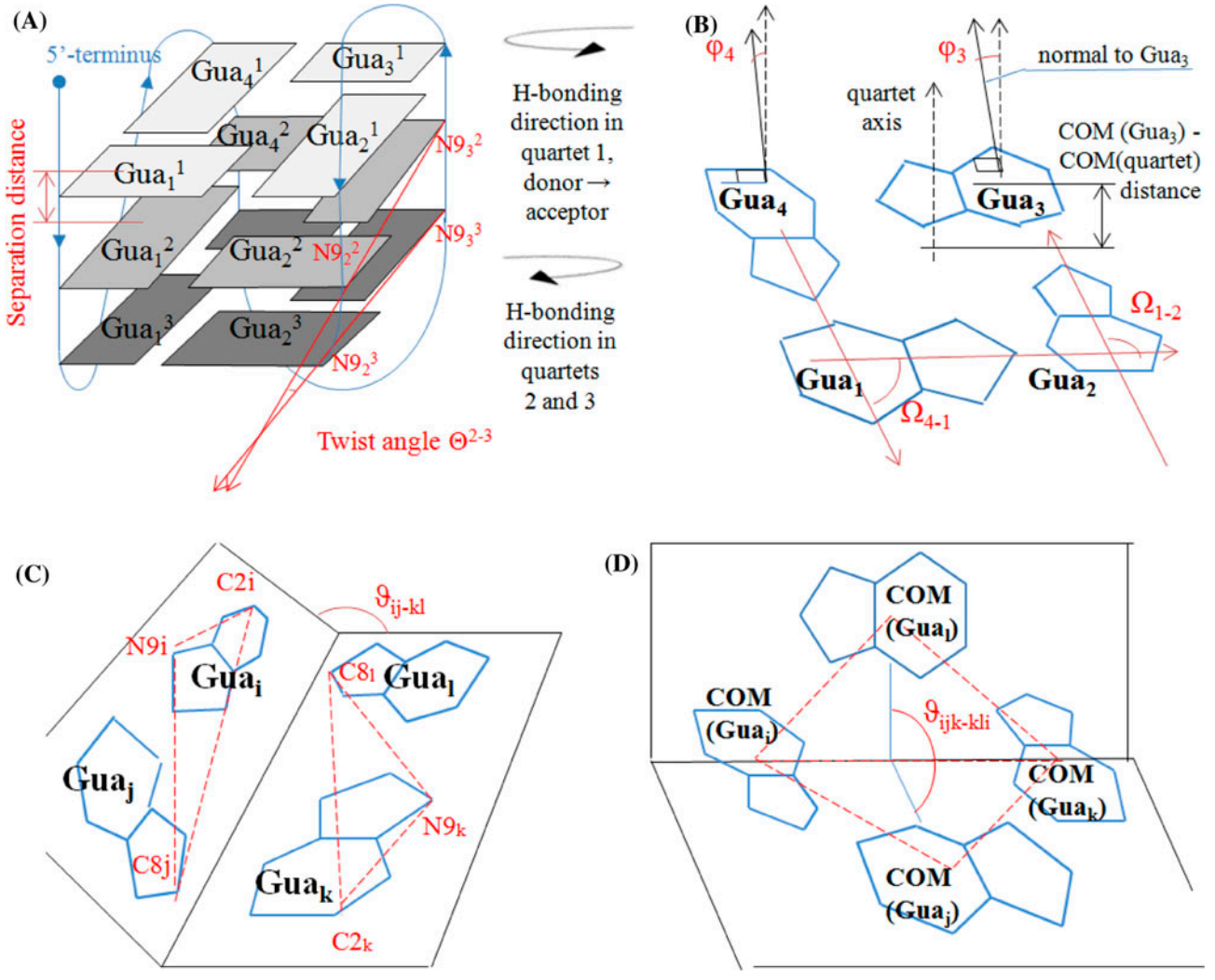


Figure 1. GQ-related parameters and the basic types of quartet bending.
(A) Schematic representation of the hybrid-1 telGQ core and parameters that indicate relative quartet positions. (B) Parameters that indicate relative Gua positions in a particular quartet. (C) Typical "lengthwise" quartet bending. (D) Typical "diagonal" quartet bending.

in accordance with quartet 1 (e.g. the guanine stacked with $Gua_1^1$ (the first guanine in quartet 1) will also be the 1st in quartet 2 ($Gua_1^2$) and so forth). Here and below, the lower index of a guanine residue, particular atom or relative parameter indicates the guanine's position in a quartet, while the upper index is a quartet number. For example, $Gua_2^3$ is the second Gua in quartet 3 and $N9_2^3$ is N9 in $Gua_2^3$.

First, we suggest using a gyration radius (the known parameter) to illustrate major structural distortions as an alternative or in addition to the commonly used parameter RMSD; the gyration radius can be estimated for the entire GQ or a particular quartet. A dramatic increase in this parameter indicates GQ/quartet collapse. Thus, a time plot of the gyration radius provides a general approximation of the MD trajectory.

Next, for a more detailed analysis, we suggest 6 basic subsets of parameters that indicate relative quartet positions (Figure 1(A); parameters 1 and 2) and motions in each particular quartet (Figure 1(B); parameters 3–6).

(1) The distance between the quartet COMs, which is also referred to as the "separation distance" (Lech et al., 2013). It is usually equal to 3.5 Å unless some major GQ distortions occur.
(2) The twist angle (Θ).

The twist angle for quartets $\alpha$ and $\beta$ is the angle between the vectors $N9_i^{\alpha}$-$N9_{i+1}^{\alpha}$ and $N9_i^{\beta}$-$N9_{i+1}^{\beta}$ irrespectively of the quartet polarity. Each twist angle is the average of four values ($i$ = 1–3 is the Gua number in a quartet; the fourth pair is $N9_1$–$N9_4$).

The twist angle depends significantly on the type of stacking interactions (Syn vs. Anti Gua conformations) and thus takes different values for quartet pairs with similar and opposite polarities (Lech et al., 2013). In our numeration system, it is typically close to 10° (Anti-Syn stacking) or 40° (Syn-Anti stacking) in the case of the opposite quartet polarities and approximately 25–30° in the case of similar polarities (Anti-Anti). The comparison of the separation distances and twist angles for several well-known GQ structures, available in PDB, is presented in the Supplementary material, Table S1.

(3) The dihedral angle of four N1 atoms.

This parameter is basically similar to that proposed by Mashimo, Yagi, Sannohe, Rajendran, and Sugiyama (2010) (i.e. the dihedral angle of four O6 atoms);

(4) The distances between the quartet COM and COMs of particular guanines or the COM(GQ)–COM(Gua) distances;
(5) The angles between the normals to the Gua planes and the axis of a quartet ($\varphi$) or the angle between the normals to Gua (delta $\varphi$). The axis of a quartet is the vector that joins its COM with the COM of a neighbouring quartet. It does not coincide with a normal to a quartet. In the case of telGQ, the axis of quartet 1 joins the COMs of quartets 1 and 2. The axis of quartet 2 coincides with the axis of quartet 3 and joins their COMs.

The parameters $\varphi$ and delta $\varphi$ indicate the relative orientations of all guanines in a quartet plane and, therefore, are more informative than previously reported planarity-related parameters, i.e. COM(N9-tetragon)–COM(O6-tetragon) distances (Reshetnikov, Golovin, Spiridonova et al., 2010) and RMSDs in the axis perpendicular to the quartet plane (Zhu et al., 2013).

(6) The angles between Gua axes (Ω). The Gua axis is the vector that joins the middle of the C4–C5 interval with the C8 atom. Ω indicates relative Gua rotation and is normally equal to ~90° for neighbouring guanines and ~180° for non-neighbouring guanines.

We additionally propose specific characteristics of particular types of quartet plane bending. Thus far, only "tepee-like" bending has been described in detail (Reshetnikov, Golovin, & Kopylov, 2010). The parameters used by Reshetnikov et al. (i.e. the COM(N9-tetragon)–COM(O6-tetragon) distances) appear reasonable and convenient for monitoring this type of quartet plane deformation. Herein, we describe "lengthwise" (Figure 1(C)) and "diagonal" (Figure 1(D)) quartet bending.

"Lengthwise" bending implies that two pairs of neighbouring guanines are approximately planar. For instance, in Figure 1(C), $Gua_i$ is approximately coplanar with $Gua_j$, and $Gua_k$ is approximately coplanar with $Gua_l$. The vectors $N9_i$–$C2_i$ and $N9_i$–$C8_j$ lie in the nominal $Gua_iGua_j$ plane. The vectors $N9_k$–$C2_k$ and $N9_k$–$C8_l$ lie in the nominal $Gua_kGua_l$ plane. Alternative "nominal planes" could be constructed using relative Gua COMs and the quartet COM. However, that approach would produce understated values of the angle between the nominal planes. "Diagonal" quartet bending implies that two non-neighbouring guanines are coplanar, but both or one of the other two guanines deviate. For instance, in Figure 1(D), $Gua_j$ is coplanar with $Gua_k$; $Gua_l$/$Gua_j$ or both deviate. The vectors that join the COMs of $Gua_i$, $Gua_j$ and $Gua_k$ lie in the $Gua_iGua_jGua_k$ nominal plane. The vectors that join the COMs of $Gua_k$, $Gua_l$ and $Gua_i$ lie in the $Gua_kGua_lGua_i$ nominal plane. The angle ($\vartheta$) between the nominal planes formed by Gua pairs or triads indicates "lengthwise" or "diagonal" quartet bending, respectively. In the latter case, this parameter is somewhat similar to the N1 dihedral angle.

### *Quantitative evaluation of conformational rearrangements in GQs*

On the basis of the above parameters, we propose the following systematic approach to describing GQ dynamics with a focus on conformational changes in the GQ core.

(1) General characterisation of major structural changes (parameters: RMSD and gyration radii ($R_g$) of the quartets and the whole GQ).

$$R_g = \sqrt{\frac{1}{N}\sum_{i=1}^{N}\left(\vec{r}_i - \vec{R}\right)^2}, \tag{1}$$

$$\vec{R} = \frac{\sum_{i=1}^{N} m_i \vec{r}_i}{\sum_{i=1}^{N} m_i}, \tag{2}$$

where $\vec{r}_i$ is the radius vector of atom $i$, $m_i$ is its mass, $N$ is a number of atoms in the quartet (for $R_g^{\text{quartet}}$) or in the whole GQ (for $R_g^{\text{GQ}}$), and $\vec{R}$ is the radius vector of the quartet COM (for $R_g^{\text{quartet}}$) or GQ COM (for $R_g^{\text{GQ}}$)

(2) Analysis of relative quartet positions (parameters: the separation distance (COM distance) and the twist angle Θ).

$$\text{COM}^{\alpha} - \text{COM}^{\beta} = || \vec{R}^{\alpha} - \vec{R}^{\beta} ||, \tag{3}$$

$$\Theta^{\alpha\beta} = \left(\Theta_{12}^{\alpha\beta} + \Theta_{23}^{\alpha\beta} + \Theta_{34}^{\alpha\beta} + \Theta_{41}^{\alpha\beta}\right)/4, \tag{4}$$

$$\Theta_{ij}^{\alpha\beta} = \frac{180}{\pi}\arccos\left(\frac{\vec{r}_{ij}^{\alpha}}{|| \vec{r}_{ij}^{\alpha} ||} \times \frac{\vec{r}_{ij}^{\beta}}{|| \vec{r}_{ij}^{\beta} ||}\right), \tag{5}$$

where $\alpha$ and $\beta$ are quartet numbers, and $\vec{r}_{ij}$ is the vector that joins N9 atoms of $\text{Gua}_i$ and $\text{Gua}_j$ in the respective quartet.

(3) Analysis of motions within a quartet (parameters: the distances between the Gua COMs COM(Gua)–COM (GQ) or COM(Gua)–COM(quartet), the angles between the Gua planes ($\varphi$ or delta $\varphi$), the dihedral angle of the N1 atoms and the angles between Gua axes).

The dihedral angle (Ξ) of the N1 atoms:

$$\Xi = \frac{180}{\pi}\arccos\left(\vec{n}_{ijk} \cdot \vec{n}_{jkl}\right), \tag{6}$$

$$\vec{n}_{ijk} = \left[\frac{\vec{r}_{ij}}{|| \vec{r}_{ij} ||} \times \frac{\vec{r}_{jk}}{|| \vec{r}_{jk} ||}\right] \tag{7}$$

where $\vec{r}_{ij}$ is the vector that joins N1 atoms of $\text{Gua}_i$ and $\text{Gua}_j$.

The angle between the normal to $\text{Gua}_i^{\alpha}$ ($\vec{n}_i$) and the axis $\vec{Z}^{\alpha\beta}$:

$$\varphi_i = \frac{180}{\pi}\arccos\left(\vec{n}_i \cdot \frac{\vec{Z}^{\alpha\beta}}{|| \vec{Z}^{\alpha\beta} ||}\right), \tag{8}$$

$$\vec{n}_i = \left[\frac{\vec{r}_{\text{N9N2}}^{\,i}}{|| \vec{r}_{\text{N9N2}}^{\,i} ||} \times \frac{\vec{r}_{\text{N9O6}}^{\,i}}{|| \vec{r}_{\text{N9O6}}^{\,i} ||}\right], \tag{9}$$

where $\vec{Z}^{\alpha\beta}$ is the vector that joins COM of quartet $\alpha$ with the COM of the neighbouring quartet $\beta$, $\vec{r}_{\text{N9N2}}^{\,i}$ is the vector that joins N9 and N2 atoms in $\text{Gua}_i^{\alpha}$, and $\vec{r}_{\text{N9O6}}^{\,i}$ joins N9 and O6 atoms in $\text{Gua}_i^{\alpha}$.

The angle between the normals to $\text{Gua}_i$ and $\text{Gua}_j$:

$$\text{delta}\,\varphi_{ij} = \frac{180}{\pi}\arccos\left(\vec{n}_i \cdot \vec{n}_j\right). \tag{10}$$

The angle between the axes of $\text{Gua}_i$ and $\text{Gua}_j$:

$$\Omega_{i-j} = \frac{180}{\pi}\arccos\left(\frac{\vec{r}_{\text{C4C5-C8}}^{\,i}}{|| \vec{r}_{\text{C4C5-C8}}^{\,i} ||} \cdot \frac{\vec{r}_{\text{C4C5-C8}}^{\,j}}{|| \vec{r}_{\text{C4C5-C8}}^{\,j} ||}\right), \tag{11}$$

where $\vec{r}_{\text{C4C5-C8}}^{\,i}$ is the vector that joins the middle of the C4–C5 interval with the C8 atom in $\text{Gua}_i$, and $\vec{r}_{\text{C4C5-C8}}^{\,j}$ joins the middle of the C4–C5 interval with the C8 atom in $\text{Gua}_j$.

(4) Analysis of quartet bending type (parameters: the angles ($\vartheta$) between nominal planes formed by Gua pairs and triads).

(4.1.) "Lengthwise" bending (the nominal planes are $\text{Gua}_i\text{Gua}_j$ and $\text{Gua}_k\text{Gua}_l$).

$$\vartheta_{ij-kl} = \frac{180}{\pi}\arccos\left(\vec{n}_{ij} \cdot \vec{n}_{kl}\right), \tag{12}$$

$$\begin{aligned}\vec{n}_{ij} &= \left[\frac{\vec{r}_{\text{N9C2}}^{\,i}}{|| \vec{r}_{\text{N9C2}}^{\,i} ||} \times \frac{\vec{r}_{\text{N9C8}}^{\,ij}}{|| \vec{r}_{\text{N9C8}}^{\,ij} ||}\right], \vec{n}_{kl} \\ &= \left[\frac{\vec{r}_{\text{N9C2}}^{\,k}}{|| \vec{r}_{\text{N9C2}}^{\,k} ||} \times \frac{\vec{r}_{\text{N9C8}}^{\,kl}}{|| \vec{r}_{\text{N9C8}}^{\,kl} ||}\right],\end{aligned} \tag{13}$$

where $\vec{n}_{ij}$ and $\vec{n}_{kl}$ are normals to the nominal planes $\text{Gua}_i$-$\text{Gua}_j$ and $\text{Gua}_k\text{Gua}_l$, respectively; $\vec{r}_{\text{N9C2}}^{\,i}$ is the vector that joins N9 and C2 atoms in $\text{Gua}_i$; $\vec{r}_{\text{N9C2}}^{\,k}$ joins N9 and C2 atoms in $\text{Gua}_k$; $\vec{r}_{\text{N9C8}}^{\,ij}$ joins $\text{N9}_i$ with $\text{C8}_j$, and $\vec{r}_{\text{N9C8}}^{\,kl}$ joins $\text{N9}_k$ with $\text{C8}_l$.

(4.2.) "Diagonal" bending (the nominal planes are $\text{Gua}_i\text{Gua}_j\text{Gua}_k$ and $\text{Gua}_k\text{Gua}_l\text{Gua}_i$).

$$\vartheta_{ijk-kli} = \frac{180}{\pi}\arccos\left(\vec{n}_{ijk} \cdot \vec{n}_{kli}\right), \tag{14}$$

$$\vec{n}_{ijk} = \left[\frac{\vec{r}_{ij}}{|| \vec{r}_{ij} ||} \times \frac{\vec{r}_{jk}}{|| \vec{r}_{jk} ||}\right], \vec{n}_{kli} = \left[\frac{\vec{r}_{kl}}{|| \vec{r}_{kl} ||} \times \frac{\vec{r}_{li}}{|| \vec{r}_{li} ||}\right] \tag{15}$$

where $\vec{n}_{ijk}$ and $\vec{n}_{kli}$ are normals to the nominal planes $\text{Gua}_i\text{Gua}_j\text{Gua}_k$ and $\text{Gua}_k\text{Gua}_l\text{Gua}_i$, respectively; $\vec{r}_{ij}$ is the vector that joins COMs of $\text{Gua}_i$ and $\text{Gua}_j$; $\vec{r}_{jk}$ is the vector that joins COMs of $\text{Gua}_j$ and $\text{Gua}_k$, etc.

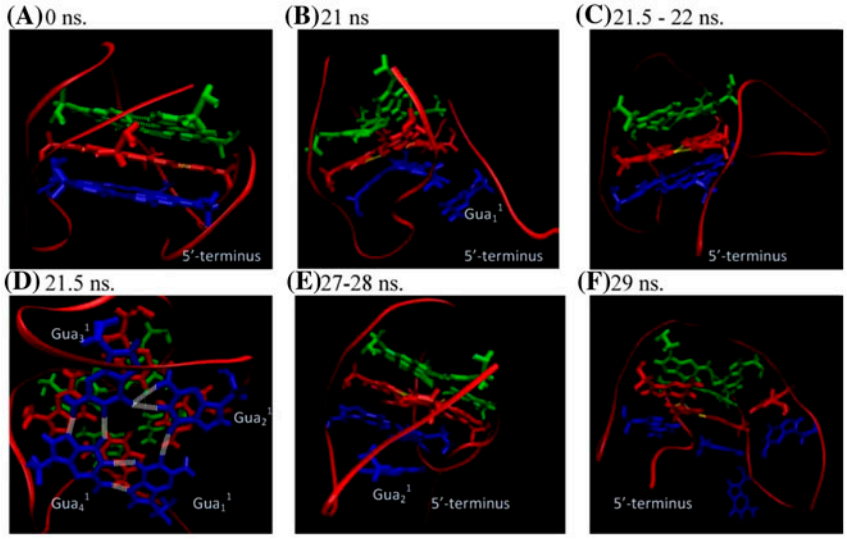


Figure 2. TelGQ MD simulation snapshots.
Notes: Quartet 1 is blue, quartet 2 is red and quartet 3 is green. (A) 0 ns. The quartets are intact and parallel. (B) 21 ns. $Gua_1^1$ deviates from the quartet 1 plane. (C) 21.5–22 ns. Quartet 1 recovers its planarity. (D) H-bonding at 21.5 ns. Despite the recovered planarity, certain changes (H-bonding rearrangements) in quartet 1 are evident. (E) 27–28 ns. $Gua_2^1$ deviates from the quartet 1 plane. (F) 29 ns. Complete disruption in quartet 1 and bending in quartets 2 and 3.

By comparing time plots for the above parameters, one can distinguish between particular types of GQ motions or estimate their relative contributions to GQ distortion. For instance, significant fluctuations in Ω and/or Gua COM distance plots, but not in $\varphi$ and N1 dihedral angle plots, indicate in-plane quartet motions. If the Gua COM distance, Ω and the N1 dihedral angle fluctuate, while $\varphi$ remains constant, the Gua deviates from but remains parallel to the quartet plane. N1 dihedral angle and/or $\varphi$ fluctuations without significant COM fluctuations indicate quartet bending without disruption.

We illustrate this approach by the analysis of telGQ dynamics.

### *Application of the new parameters for the analysis of GQ MD trajectory*

A 34 ns MD simulation was performed for the hybrid-1 telGQ (the schematic representation is given in Figure 1(A)). Despite the relatively low energetic barrier between the two hybrid telGQ conformations, we did not observe hybrid-2 formation, mainly because the simulation time was limited. NMR data indicate that interconversion is slow (Dai, Carver, Punchihewa, Jones, & Yang, 2007). Nevertheless, we observed certain conformational changes that indicate the beginning of major rearrangements (Figure 2).

At 0 ns (Figure 2(A)), the quartets were planar, and each quartet was stabilised by 8 H-bonds. During the first 20 ns, we only observed minor fluctuations, such as moderate quartet bending and reversible H-bonding disruption. Major quartet distortions were observed at approximately 21–22 ns and 27–30 ns. At 21 ns, fluctuations in quartet 1 yielded significant deviation and, finally, bulging of $Gua_1^1$ (Figure 2(B)). Theoretically, this could indicate the beginning of detachment of the 5′-terminal G-track from the GQ core, which is considered the primary pathway for hybrid-1 → hybrid-2 interconversion via the intermediate triplex structure (Mashimo et al., 2010). However, in our simulation, $Gua_1^1$ bulging was reversible, and at 22 ns, quartet 1 recovered its planarity (Figure 2(C)); however, its H-bonds were substantially rearranged (Figure 2(D)). The $NH(G_1^1)$–$O6(G_2^1)$ bond was broken, and the $NH_2(G_2^1)$–$O6(G_3^1)$ bond formed instead of the $NH_2(G_2^1)$–$N7(G_3^1)$ bond. Thereafter, $Gua_2^1$ lost its H-bonds with the neighbouring guanines, which led to $Gua_2^1$ bulging from the quartet at 27–28 ns (Figure 2(E)). At 29 ns, quartet 1 was fully disintegrated, and the remaining two quartets underwent bending (Figure 2(F)). At 30 ns, telGQ almost returned to its 28-ns conformation; however, thereafter, telGQ fully collapsed due to increasing fluctuation.

The telGQ MD trajectory was described quantitatively using the proposed algorithm.

Time plots of the gyration radii, which provide a general estimation of telGQ integrity; separation distances and twist angles, which indicate relative quartet positions, and the N1 dihedral angels, which allow for the rough assessment of quartet planarity, are shown in Figure 3.

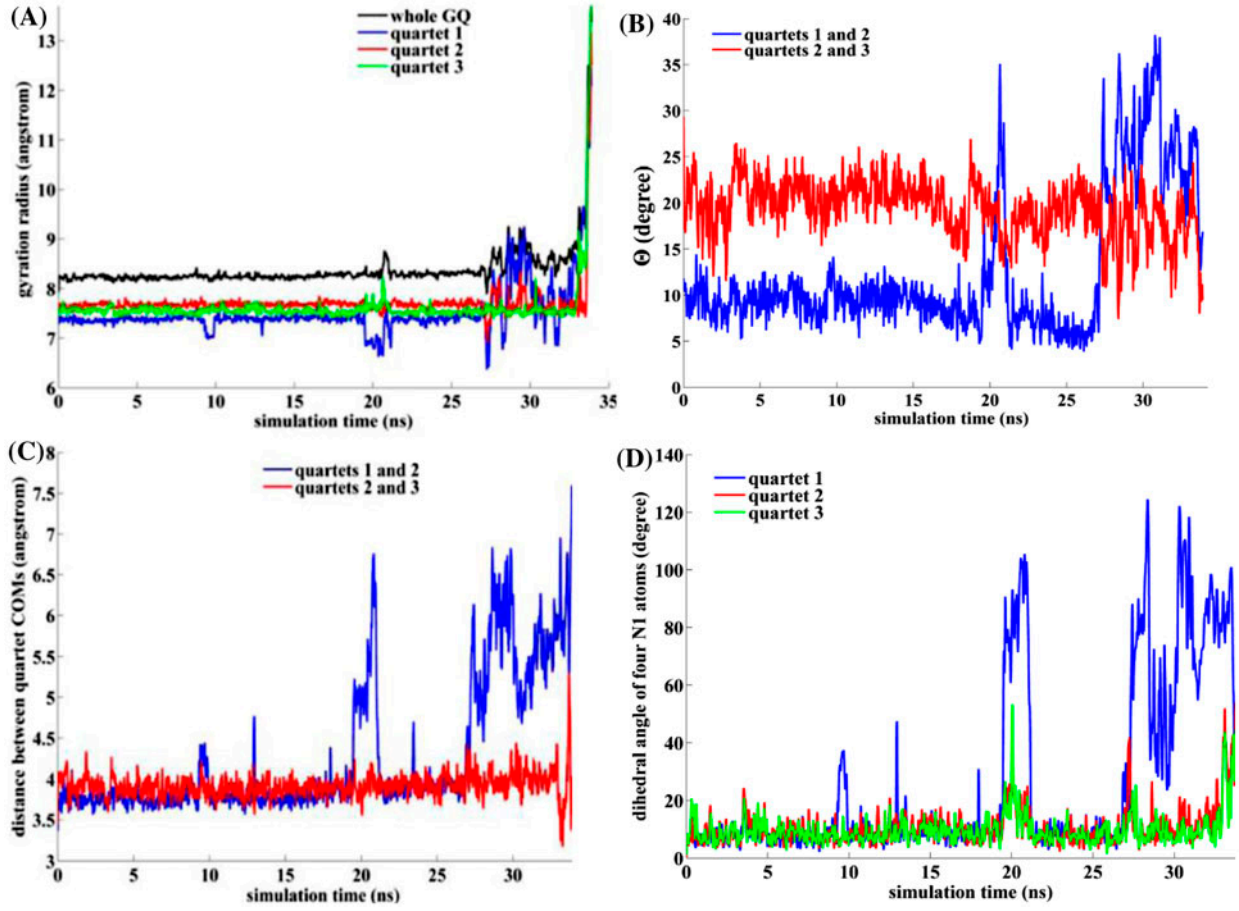


Figure 3. Basic GQ-related parameters and their fluctuations during a telGQ MD simulation.
(A) gyration radii; (B) twist angles; (C) distances between quartet COMs; (D) the dihedral angles of the N1 atoms in each of the three quartets.

The plots of COM(Gua)–COM(quartet) distances and $\varphi$ angles, which illustrate the changes of quartet integrity and planarity, respectively, are shown in Figure 4. (For the COM(Gua)–COM(GQ) plots and delta $\varphi$ plots, see Supplementary material, Figure S1). Figure 5 illustrates "diagonal" and "lengthwise" bending of telGQ quartets.

Moderate gyration radii fluctuations at approximately 21–22 ns (Figure 3(A)) indicate reversible quartet distortions. Major fluctuations at 27–28 ns suggest substantial conformational changes that lead to a dramatic increase in the gyration radii after 30 ns, which indicates GQ collapse. The separation distance fluctuations at 21 ns (Figure 3(C), quartets 1 and 2) might appear to indicate mutual quartet divergence; however, as we show below, this is actually not the case. Quartet 1 does not deviate from quartet 2; only particular guanines move out of the quartet plane, and the plane bends significantly, which is evident from the N1 dihedral angle plot (Figure 3(D)).

The COM distance plots, N1 dihedral angle plots and $\varphi$ plots in Figures 3 and 4 clearly illustrate the following conformational changes in telGQ: $Gua_1^1$ deviation from quartet 1 at approximately 21 ns; $Gua_2^1$ deviation from quartet 1 at approximately 27 ns and subsequent collapse of quartet 1 with simultaneous bending in quartets 2 and 3.

The disrupted integrity of quartet 1 at 21–22 ns and after 27 ns is evident in Figure 4(A) and (D). The maximum COM(Gua)–COM(quartet) (Figure 4(A)) and COM (Gua)–COM(GQ) (Figure S1(A)) distances were observed for $Gua_1^1$ (21–22 ns) and $Gua_2^1$ (27–28 ns). The absence of substantial fluctuations at 21–22 ns in the quartet 1 $\varphi$ plots (Figure 4(D)) indicates that $Gua_1^1$ deviates from but remains parallel to the quartet plane (which is also evident in the 22-ns MD snapshot, Figure 2(B)). After 27 ns, all $\varphi$ fluctuations in quartet 1 increased (Figure 4(D)), and the maximum amplitude was observed for $Gua_2^1$. In the delta $\varphi$ plots (Figure S1(D)), maximum amplitudes were observed for the pairs $Gua_1^1$–$Gua_2^1$, $Gua_2^1$–$Gua_3^1$ and $Gua_2^1$–$Gua_4^1$. The latter observations indicate that $Gua_2^1$ not only deviates from but also rotates out of the quartet plane (Figure 2(F)). The fluctuations in quartets 2 and 3 are relatively small compared with

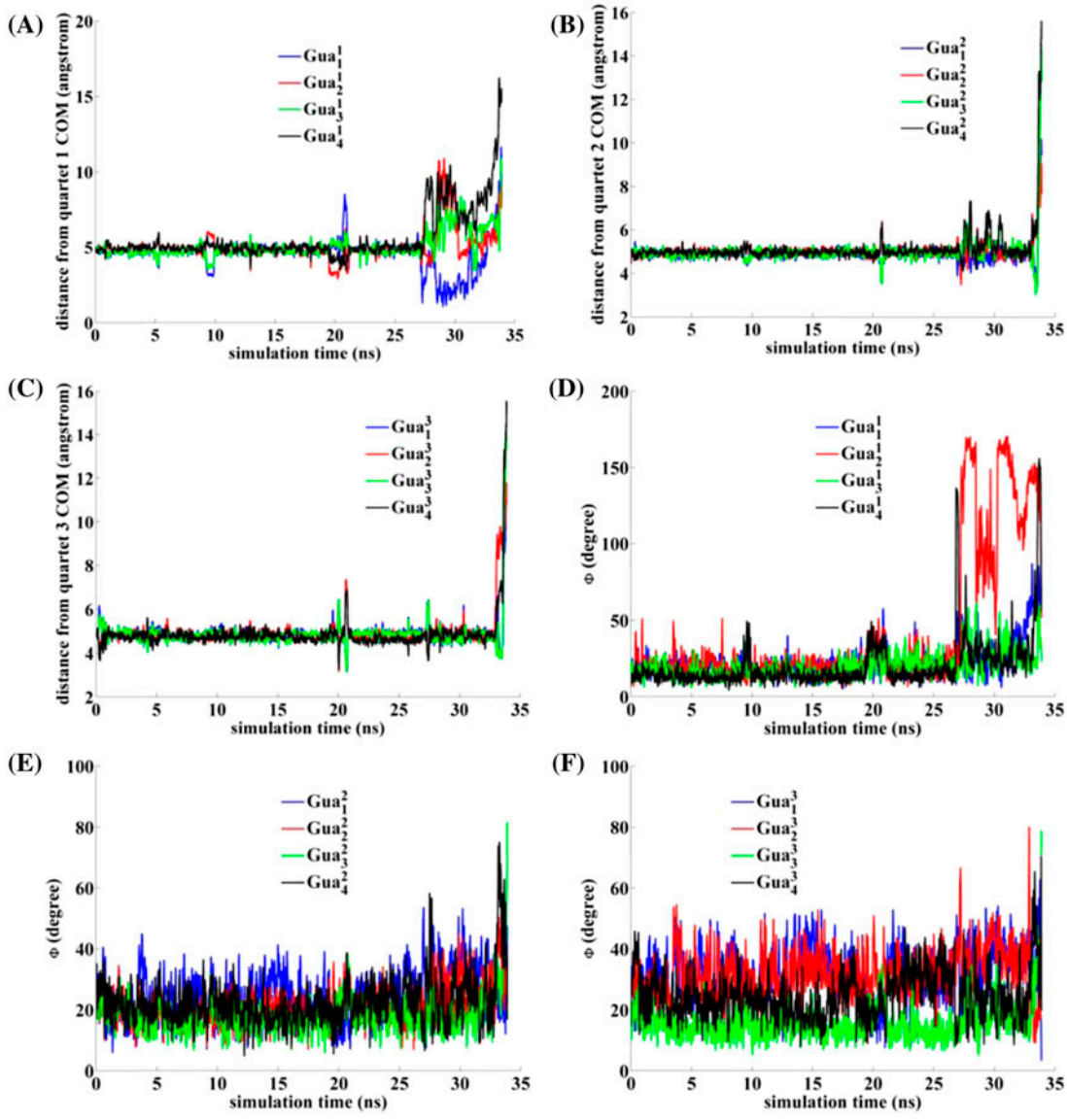


Figure 4. Parameters that describe quartet integrity (A–C) and planarity (D–F) in telGQ.
(A–C) Distances between the quartet COM and COMs of particular guanines; (D–F) angles between the normals to the Gua planes in a particular quartet and the axis of the quartet.

quartet 1 until 27 ns. Figure 4(B) and (C) illustrates the integrity of quartets 2 and 3, and their planarity is most evident in Figure 3(D). Figure 4(E) and (F) illustrates a gradual increase in the relative Gua plane inclination. Apparently, quartet 2 is the least flexible.

Relative rotation of the guanines (Ω deviation from the normal values) was insignificant in all quartets until 27 ns, when major distortions began (Supplementary material, Figure S2). Mixed "lengthwise"/"diagonal" bending was of quartets 1 and 2 (especially quartet 1) after 27 ns is evident from Figure 5(A) and (B).

The new set of GQ core-related parameters is clearly applicable not only to natural DNA/RNA GQs but also their analogues with artificial loops (e.g. various chemically modified GQ aptamers and their complexes with proteins or small molecule ligands). In our recent study, we described the conformation and dynamics of a modified thrombin-binding aptamer, triazole–TBA, in complex with thrombin. Triazole–TBA is an active thrombin inhibitor with enhanced resistance to nuclease hydrolysis due to a non-natural triazole internucleotide linkage in a central loop of the two-tetrad antiparallel GQ structure (Sequence: d[GGTTGGTT*TGGTTGG], * is a triazole internucleotide linkage).

Molecular dynamics simulations were used to predict the most likely triazole–TBA/thrombin-binding mode. Two models of the aptamer/protein complex were considered: model 1, in which the aptamer binds the

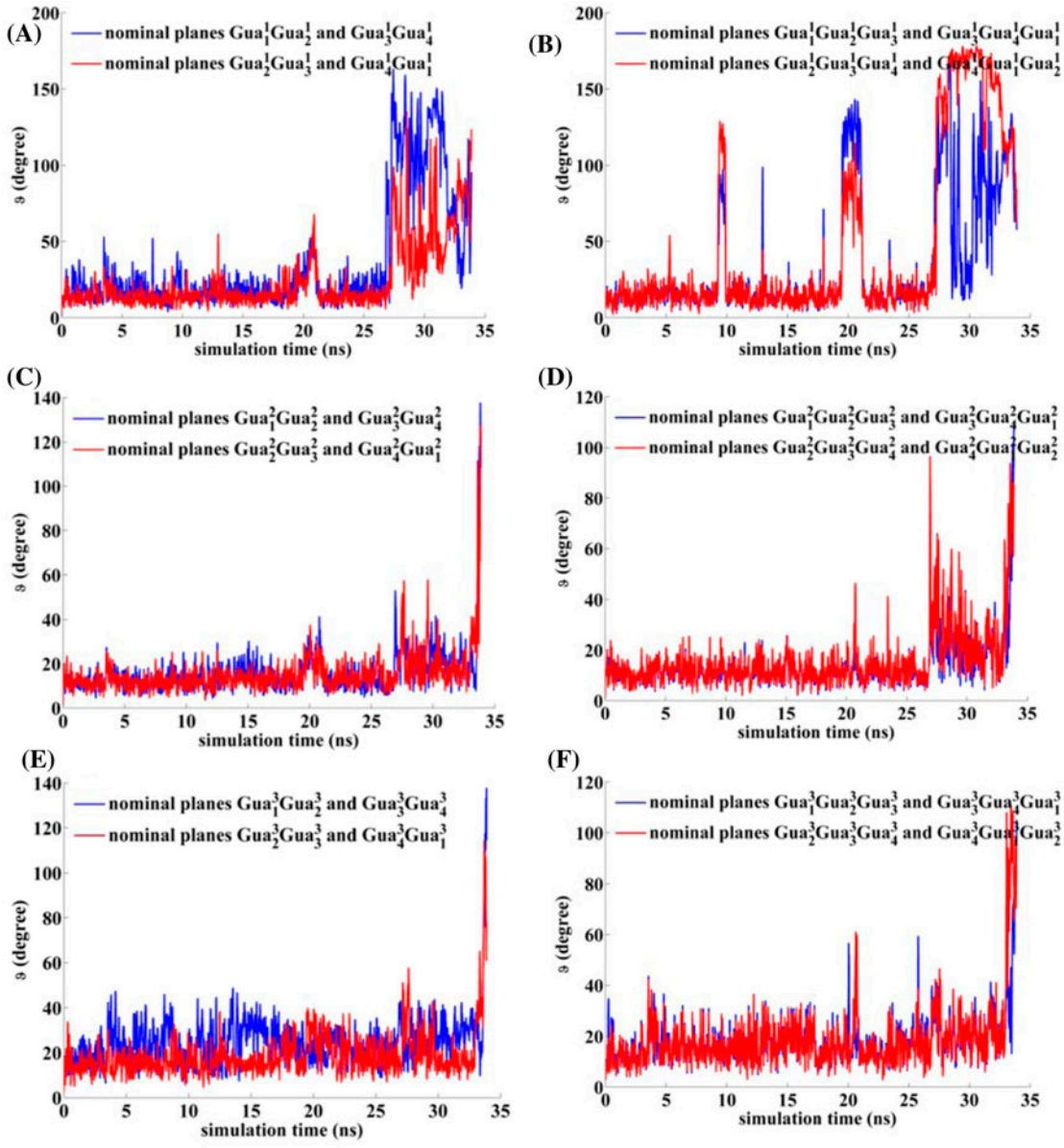


Figure 5. The angles between nominal planes formed by the Gua pairs and triads that characterise telGQ quartet bending. (A) "Lengthwise" quartet 1 bending. (B) "Diagonal" quartet 1 bending. (C) "Lengthwise" quartet 2 bending. (D) "Diagonal" quartet 2 bending. (E) "Lengthwise" quartet 3 bending. (F) "Diagonal" quartet 3 bending.

thrombin exosite-1 through the TT loops, and model 2, in which the modified (TT*T) loop participates in the binding. The triazole–TBA models 1 and 2 were constructed using NMR and XRD structures of the unmodified TBA, PDB:1HAO and PDB:1HUT, respectively. MD simulation results suggest that model 1 is valid; the GQ was stable and did not dissociate from the protein throughout the 35 ns dynamics simulation, but in model 2, we observed significant deformation of the GQ core. Details on the triazole–TBA interaction with thrombin are described in (Varizhuk et al., 2013). Here, we focused on GQ conformational changes in models 1 and 2.

Figure S3 (Supplementary material) shows MD simulation snapshots that illustrate the major deformations of triazole–TBA GQ in complex with thrombin; the new set of parameters was used to monitor, illustrate and analyse those deformations. In general, triazole–TBA model 1 underwent only minor changes (i.e. insignificant "lengthwise" bending in quartet 2 at approximately 9.5 ns (Figure S3(B)) and in quartet 1 at approximately 30 ns (Figure S3(C))). Alternatively, in model 2, the quartet planarity was severely distorted (Figures S3(F–H) and S4). Major fluctuations began at approximately 27 ns (Figures S2(F), S4 and S5(B) and (D)). The $\varphi$ and delta

$\varphi$ plots clearly show that $Gua_2^1$ and $Gua_3^1$ turned away/rotated from quartet 1 (Figure S6(E) and (G)), and $Gua_3^2$ deviated from quartet 2 (Figure S6(F) and (H)). Profound "lengthwise" bending of quartets 1 and 2 was observed at 33 ns (Figure S7(C) and (D)); at the end of the simulation, most binding contacts with the protein were lost.

## Conclusion

We described a systematic approach to discerning conformational changes in GQs based on a consecutive characterisation of GQ core integrity in general, the relative orientation of G-quartets and the motions in each quartet. New quartet integrity- and quartet planarity-related parameters were developed. Taken together, these characterisations will aid in discriminating between particular types of quartet deformation (e.g. bulging of a single guanine, inclination of a single-guanine, tepee- or wedge-like bending of a quartet.). The advantages of the new parameters were demonstrated using hybrid-1 telGQ and TBA, but they may be applied to any GQ structure.

## Supplementary material

Supplementary material dealing with the comparison of relative quartet positions in different GQ types (Table S1), quartet integrity and polarity in telGQ (Figure S1), relative Gua rotation in telGQ (Figure S2), MD simulation for triazole-TBA (Figure S3) and quartet integrity/planarity in triazole-TBA (Figures S4-S7) in addition to detailed instructions for using the VMD scripts is available online at: http://dx.doi.org/10.1080/07391102.2015.1055303.

VMD scripts for calculating all GQ-related parameters are available from the authors at: http://niifhm.ru/wp-content/uploads/2015/04/VMD_script_for_describing_2_tetrad_GQs.txt; http://niifhm.ru/wp-content/uploads/2015/04/VMD_script_for_describing_3_tetrad_GQs.txt; http://niifhm.ru/wp-content/uploads/2015/04/VMD_script_for_describing_4_tetrad_GQs.txt

## Disclosure statement

No potential conflict of interest was reported by the authors.

## Funding

This work was supported by the Russian Science Foundation [grant number 14-25-00013]; Dinasty Foundation fellowship to A.V.; Russian Foundation for Basic Research [grant number 14-04-01244].

## References

Bashford, D. & Case, D. A. (2000). Generalized Born models of macromolecular solvation effects. *Annual Review of Physical Chemistry, 51*, 129–152.

Blanchet, C., Pasi, M., Zakrzewska, K., & Lavery, R. (2011). CURVES+ web server for analyzing and visualizing the helical, backbone and groove parameters of nucleic acid structures. *Nucleic Acids Research, 39*, W68–W73.

Bochman, M. L., Paeschke, K., & Zakian, V. A. (2012). DNA secondary structures: Stability and function of G-quadruplex structures. *Nature Reviews Genetics, 13*, 770–780.

Burge, S., Parkinson, G. N., Hazel, P., Todd, A. K., & Neidle, S. (2006). Quadruplex DNA: Sequence, topology and structure. *Nucleic Acids Research, 34*, 5402–5415.

Cang, X., Sponer, J., & Cheatham, T. E., III. (2011). Explaining the varied glycosidic conformational, G-tract length and sequence preferences for anti-parallel G-quadruplexes. *Nucleic Acids Research, 39*, 4499–4512.

Colasanti, A. V., Lu, X. J., & Olson, W. K. (2013). Analyzing and building nucleic acid structures with 3DNA. *Journal of Visualized Experiments, 74*, 4401.

Dai, J., Carver, M., Punchihewa, C., Jones, R. A., & Yang, D. (2007). Structure of the Hybrid-2 type intramolecular human telomeric G-quadruplex in $K^+$ solution: Insights into structure polymorphism of the human telomeric sequence. *Nucleic Acids Research, 35*, 4927–4940.

Gray, R. D., Trent, J. O., & Chaires, J. B. (2014). Folding and unfolding pathways of the human telomeric G-quadruplex. *Journal of Molecular Biology, 426*, 1629–1650.

Haider, S., & Neidle, S. (2010). Molecular modeling and simulation of G-quadruplexes and quadruplex-ligand complexes. *Methods in Molecular Biology, 608*, 17–37.

Humphrey, W., Dalke, A., & Schulten, K. (1996). VMD: Visual molecular dynamics. *Journal of Molecular Graphics, 14*, 27–38.

Lane, A. N., Chaires, J. B., Gray, R. D., & Trent, J. O. (2008). Stability and kinetics of G-quadruplex structures. *Nucleic Acids Research, 36*, 5482–5515.

Lech, C. J., Heddi, B., & Phan, A. T. (2013). Guanine base stacking in G-quadruplex nucleic acids. *Nucleic Acids Research, 41*, 2034–2046.

Li, M.-H., Luo, Q., Xue, X.-G., & Li, Z.-S. (2010). Toward a full structural characterization of G-quadruplex DNA in aqueous solution: Molecular dynamics simulations of four G-quadruplex molecules. *Journal of Molecular Structure: THEOCHEM, 952*, 96–102.

Luu, K. N., Phan, A. T., Kuryavyi, V., Lacroix, L., & Patel, D. J. (2006). Structure of the human telomere in $K^+$ solution: An intramolecular (3 + 1) G-quadruplex scaffold. *Journal of the American Chemical Society, 128*, 9963–9970.

Maizels, N. (2006). Dynamic roles for G4 DNA in the biology of eukaryotic cells. *Nature Structural & Molecular Biology, 13*, 1055–1059.

Mashimo, T., Yagi, H., Sannohe, Y., Rajendran, A., & Sugiyama, H. (2010). Folding pathways of human telomeric type-1 and type-2 G-quadruplex structures. *Journal of the American Chemical Society, 132*, 14910–14918.

Mukundan, V. T., & Phan, A. T. (2013). Bulges in G-quadruplexes: Broadening the definition of G-quadruplex-forming sequences. *Journal of the American Chemical Society, 135*, 5017–5028.

Murat, P., & Balasubramanian, S. (2014). Existence and consequences of G-quadruplex structures in DNA. *Current Opinion in Genetics & Development, 25*, 22–29.

Onufriev, A., Bashford, D., & Case, D. A. (2000). Modification of the generalized Born model suitable for macromolecules. *The Journal of Physical Chemistry B, 104*, 3712–3720.

Parkinson, G. N., Lee, M. P., & Neidle, S. (2002). Crystal structure of parallel quadruplexes from human telomeric DNA. *Nature, 417*, 876–880.

Petraccone, L., Spink, C., Trent, J. O., Garbett, N. C., Mekmaysy, C. S., Giancola, C., & Chaires, J. B. (2011). Structure and stability of higher-order human telomeric quadruplexes. *Journal of the American Chemical Society, 133*, 20951–20961.

Phan, A. T., Kuryavyi, V., Luu, K. N., & Patel, D. J. (2007). Structure of two intramolecular G-quadruplexes formed by natural human telomere sequences in $K^+$ solution. *Nucleic Acids Research, 35*, 6517–6525.

Phan, A. T., Luu, K. N., & Patel, D. J. (2006). Different loop arrangements of intramolecular human telomeric (3+1) G-quadruplexes in $K^+$ solution. *Nucleic Acids Research, 34*, 5715–5719.

Reshetnikov, R., Golovin, A., Spiridonova, V., Kopylov, A., & Šponer, J. (2010). Structural dynamics of thrombin-binding DNA aptamer d(GGTTGGTGTGGTTGG) quadruplex DNA studied by large-scale explicit solvent simulations. *Journal of Chemical Theory and Computation, 6*, 3003–3014.

Reshetnikov, R. V., Golovin, A. V., & Kopylov, A. M. (2010). Comparison of models of thrombin-binding 15-mer DNA aptamer by molecular dynamics simulation. *Biochemistry (Moscow), 75*, 1017–1024.

Reshetnikov, R. V., Sponer, J., Rassokhina, O. I., Kopylov, A. M., Tsvetkov, P. O., Makarov, A. A., & Golovin, A. V. (2011). Cation binding to 15-TBA quadruplex DNA is a multiple-pathway cation-dependent process. *Nucleic Acids Research, 39*, 9789–9802.

Ryckaert, J.-P., Ciccotti, G., & Berendsen, H. J. C. (1977). Numerical integration of the cartesian equations of motion of a system with constraints: Molecular dynamics of *n*-alkanes. *Journal of Computational Physics, 23*, 327–341.

Šponer, J., Cang, X., & Cheatham, T. E., III. (2012). Molecular dynamics simulations of G-DNA and perspectives on the simulation of nucleic acid structures. *Methods, 57*, 25–39.

Stadlbauer, P., Trantírek, L., Cheatham, T. E., III, Koča, J., & Šponer, J. (2014). Triplex intermediates in folding of human telomeric quadruplexes probed by microsecond-scale molecular dynamics simulations. *Biochimie, 105*, 22–35.

Varizhuk, A. M., Tsvetkov, V. B., Tatarinova, O. N., Kaluzhny, D. N., Florentiev, V. L., Timofeev, E. N., … Pozmogova, G. E. (2013). Synthesis, characterization and *in vitro* activity of thrombin-binding DNA aptamers with triazole internucleotide linkages. *European Journal of Medicinal Chemistry, 67*, 90–97.

Wang, Y., & Patel, D. J. (1993). Solution structure of the human telomeric repeat d[AG3(T2AG3)3] G-tetraplex. *Structure, 1*, 263–282.

Zhu, H., Xiao, S., & Liang, H. (2013). Structural dynamics of human telomeric G-quadruplex loops studied by molecular dynamics simulations. *PLoS One, 8*, e71380.